The Mitochondrial Acyl-carrier Protein Interaction Network Highlights Important Roles for LYRM Family Members in Complex I and Mitoribosome Assembly

Authors

Marris G. Dibley, Luke E. Formosa, Baobei Lyu, Boris Reljic, Dylan McGann, Linden Muellner-Wong, Felix Kraus, Alice J. Sharpe, David A. Stroud, and Michael T. Ryan

Correspondence

Michael.Ryan@monash.edu

In Brief

The mitochondrial acyl-carrier protein NDUFAB1 interacts with members of the LYRM (Leucine-Tyrosine-Arginine motif) family to perform a variety of functions. Here we describe the importance of two LYRM proteins in the assembly of multi-subunit mitochondrial complexes. The AltMiD51 LYRM member participates in the assembly of the mitoribosome through stabilization of the mitochondrial ribosome assembly factor MALSU1 whereas LYRM2 is required for efficient assembly of complex I through integration of the N-module.

Graphical Abstract

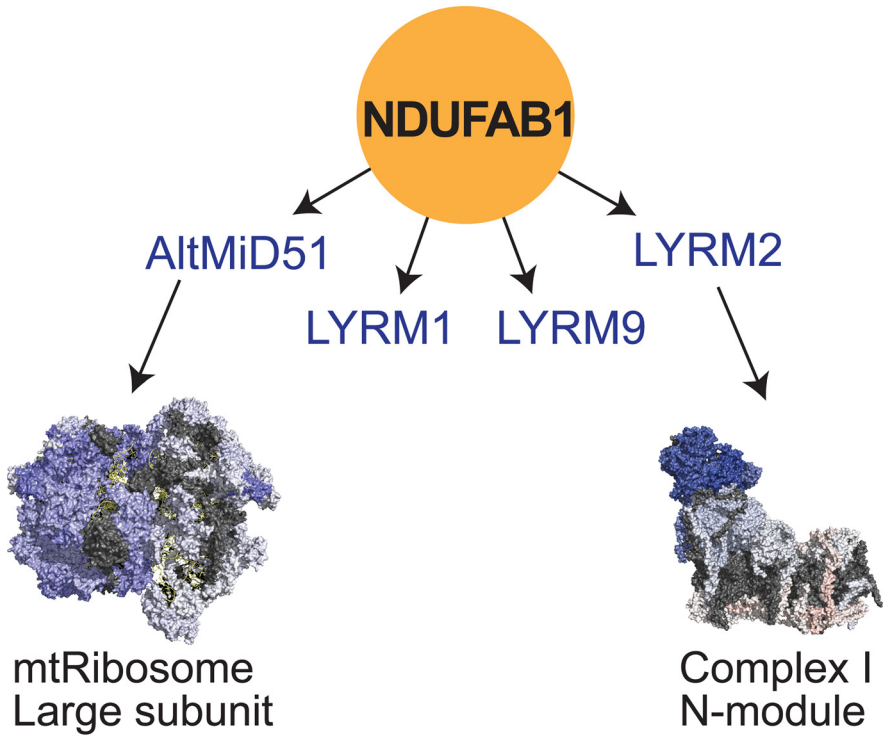

Highlights

- The interaction network of NDUFAB1 reveal associations with 9 known LYRM proteins as well as more than 20 other proteins involved in mitochondrial respiratory chain complex and mitochondrial ribosome assembly.
- The LYRM protein AltMiD51 is required for the stability of assembly factor MALSU1 and optimal assembly of the mitoribosome.
- LYRM2 is important for integration of the N-module into respiratory chain complex I.

Dibley et al., 2020, Molecular & Cellular Proteomics *19*, 65–77
January 2020
https://doi.org/10.1074/mcp.RA119.001784

The Mitochondrial Acyl-carrier Protein Interaction Network Highlights Important Roles for LYRM Family Members in Complex I and Mitoribosome Assembly*[S]

Marris G. Dibley‡‖, Luke E. Formosa‡‖, Baobei Lyu‡, Boris Reljic§, Dylan McGann‡, Linden Muellner-Wong‡, Felix Kraus‡, Alice J. Sharpe‡, David A. Stroud§, and Michael T. Ryan‡¶

NDUFAB1 is the mitochondrial acyl carrier protein (ACP) essential for cell viability. Through its pantetheine-4′-phosphate post-translational modification, NDUFAB1 interacts with members of the leucine-tyrosine-arginine motif (LYRM) protein family. Although several LYRM proteins have been described to participate in a variety of defined processes, the functions of others remain either partially or entirely unknown. We profiled the interaction network of NDUFAB1 to reveal associations with 9 known LYRM proteins as well as more than 20 other proteins involved in mitochondrial respiratory chain complex and mitochondrial ribosome assembly. Subsequent knockout and interaction network studies in human cells revealed the LYRM member AltMiD51 to be important for optimal assembly of the large mitoribosome subunit, consistent with recent structural studies. In addition, we used proteomics coupled with topographical heat-mapping to reveal that knockout of LYRM2 impairs assembly of the NADH-dehydrogenase module of complex I, leading to defects in cellular respiration. Together, this work adds to the catalogue of functions executed by LYRM family of proteins in building mitochondrial complexes and emphasizes the common and essential role of NDUFAB1 as a protagonist in mitochondrial metabolism. ***Molecular & Cellular Proteomics 19: 65–77, 2020. DOI: 10.1074/mcp.RA119.001784.***

The acyl carrier protein (ACP)[1] is a component of the type II fatty acid synthase and polyketide synthase systems found in bacteria, chloroplasts and mitochondria (1, 2). ACP can be found as a matrix soluble protein (3), where it interacts with the leucine-tyrosine-arginine motif (LYRM) containing family of proteins. This family is comprised of small (<15kDa), basic proteins, which harbor the LYRM toward the N terminus followed by a highly conserved downstream phenylalanine, typically flanked by arginine residues. ACP is essential for cell viability in both yeast and human cells where it participates with individual LYRM members in diverse processes including respiratory chain assembly and Fe-S cluster biogenesis (4–6). A pantetheine-4′-phosphate (4′-PP) prosthetic group, covalently bound at an invariant serine residue in ACP, serves as the attachment-point for acyl chains as thioesters (7). The 4′-PP is essential for LYRM protein interactions, whereas its acylation increases binding affinity (8). This suggests that the 4′-PP may act as a docking site for the interaction with the LYR motif, whereas the extending acyl chain acts like a "key in a lock" to help stabilize interactions and facilitate its activity. It was recently shown in yeast that acylation of ACP acts as an allosteric activator of LYRM family members in respiratory chain assembly through the availability of acetyl-CoA, linking free levels of the substrate with regulation of respiration (8).

In metazoans and some fungi, mitochondrial ACP (NDUFAB1 in humans), is also integrated into mitochondrial complex I (NADH-ubiquinone oxidoreductase) where it acts as an accessory/supernumerary subunit critical for assembly (4, 7). Uniquely, NDUFAB1 is found at two sites - on the distal end of the membrane arm and as a protrusion from the matrix arm (9). At these sites, NDUFAB1 directly interacts with complex I subunits NDUFB9 (membrane arm) and NDUFA6 (matrix arm) (10), both of which are also members of the LYRM family. In complex I, the 4′-PP conjugated acyl-chain of NDUFAB1 inserts into a hydrophobic channel present in both NDUFA6 and NDUFB9, whereas salt-bridge contacts are made between two conserved glutamates in NDUFAB1 and the positively charged residues of the LYRMs (10).

The full breadth of the mammalian NDUFAB1-LYRM interaction network is not yet fully known, however it is clear that

From the ‡Department of Biochemistry and Molecular Biology, Biomedicine Discovery Institute, Monash University, Melbourne, Australia; §Department of Biochemistry and Molecular Biology, The Bio21 Molecular Science & Biotechnology Institute, University of Melbourne, Melbourne, Australia

Received September 17, 2019
Published, MCP Papers in Press, October 30, 2019, DOI 10.1074/mcp.RA119.001784

NDUFAB1 interacts with LYRM4 during the biogenesis of mitochondrial Fe-S clusters in a similar fashion to that seen with NDUFB9/NDUFA6 in complex I (11). Interestingly, Fe-S biogenesis has been coupled to fatty acid synthesis via mutual interdependence on the 4′-PP (12). Similarly, LYRM5 was recently found to interact with NDUFAB1 where it is involved in deflavinating the electron transferring flavoprotein (5). Additional LYRM members involved in the assembly of other complexes of the oxidative phosphorylation (OXPHOS) machinery including complex II (13), complex III (14) and complex V (15) have also been shown to interact with NDUFAB1 (5). The functions of several other LYRM family members are yet to be characterized, and new members are also being discovered. For example, an open reading frame in the 5′ region of the transcript in the mitochondrial fission adapter MiD51 was found to encode the LYRM member AltMiD51 (16). Although AltMiD51 (also termed MIEF1-microprotein and L0R8F8) was suggested to influence mitochondrial dynamics (17), it was reported to associate with mitochondrial ribosomal subunits where it directly regulates translation (18). However, rather than direct regulation of ribosome translation activity, AltMiD51 may instead function in ribosome assembly. Structural studies of an assembly intermediate of the large mitoribosome subunit was found to contain the known assembly factor MALSU1 bound to AltMiD51 along with NDUFAB1, none of which are present in the mature ribosome (19). The importance of AltMiD51 in ribosome function therefore requires clarification. In this study, we dissect the interaction network of NDUFAB1 and investigate the interplay with partially or entirely uncharacterised LYRM family members. We establish roles for LYRM2 in complex I biogenesis, and AltMiD51 in MALSU1 stabilization and ribosome assembly.

EXPERIMENTAL PROCEDURES

Tissue Culture and SILAC Labeling—HEK293T cells were cultured in Dulbecco's modified Eagle's medium (DMEM) supplemented with 10% fetal calf serum, 1% penicillin/streptomycin, 50 μg/ml uridine and 1× Glutamax (ThermoFisher Scientific, Waltham, MA). Inhibition of mitochondrial translation was performed by the addition of 50 μg/ml chloramphenicol (Sigma, St. Louis, MO) for up to 96 h as indicated. For stable isotope labeling with amino acids in cell culture (SILAC), cells were cultured as previously described (4, 20). In short, SILAC DMEM lacking lysine and arginine (ThermoFisher Scientific) was supplemented with 600 mg/ml L-proline and 10 kDa dialyzed fetal calf serum (Sigma-Aldrich). Media additionally contained either "light" lysine and arginine (146 μg/ml L-lysine-HCl and 42 μg/ml L-arginine-HCl) or "heavy" (180 μg/ml $^{13}C_6{}^{15}N_2$-L-lysine-HCl and 44 μg/ml $^{13}C_6{}^{15}N_4$-L-arginine-HCl) (Cambridge Isotope Laboratories, Tewksbury, MA and Silantes, Munich, Germany respectively). Cells were incubated at 37 °C supplemented with 5% CO_2.

[1] The abbreviations used are: ACP, acyl carrier protein; 4′PP, pantetheine-4′-phosphate; ACN, Acetonitrile; AE-MS, Affinity-enrichment mass spectrometry; CCCP, Carbonyl cyanide m-chlorophenyl hydrazine; LFQ, Label free quantitation; LYRM, Leucine-Tyrosine-Arginine motif; OXPHOS, oxidative phosphorylation; SILAC, Stable isotope labelling with amino acids in cell culture.

Microscopy Sample Preparation—Cells were seeded 2 days before experimental manipulation on HistoGrip (ThermoFisher Scientific) coated glass coverslips. Coverslips were coated according to manufacturer's instructions. Cells were fixed with 4% paraformaldehyde in PBS for 10 min. After permeabilization with 0.5% Triton X-100 in PBS, cells were incubated with primary antibodies against Tom20 (rabbit polyclonal, 1:500, Santa Cruz, Dallas, TX, SC11415) and Flag (mouse monoclonal, 1:100, Sigma-Aldrich, F1804) for 90 min in 3% BSA, 0.02% Tween-20 in PBS at room temperature. Primary antibodies were labeled for 60 min with Alexa-Fluor-488 conjugated anti-mouse-IgG or Alexa-Fluor-568 conjugated anti-rabbit-IgG (ThermoFisher Scientific, A-11001 and A-11011, respectively) diluted in 3% BSA, 0.02% Tween-20 in PBS at room temperature. Hoechst 33258 (1 μg/ml; Sigma) was used to stain nuclei.

Microscopy—Confocal microscopy was performed on a Leica TCS SP8 confocal microscope (405 nm, 488 nm, 552 nm, 647 nm; Leica Microsystems, Wetzlar, Germany) equipped with HyD detectors using a 63×/1.40 NA oil immersion objective (HC PLAPO, CS2, Leica Microsystems). Microscopy data was recorded using the Leica LAS X Life software. Images in all experimental groups were obtained using the same settings. Z-sectioning was performed using 300 nm slices. Leica .lif files were converted to multi-color .tiff composite stacks using custom-written Fiji/ImageJ macros.

Image and Statistical Analysis—Images were analyzed using Fiji and custom-written macros (21). Correlation coefficient R, measuring the correlation of Tom20 (mitochondria) and Flag antibody staining was measured using the Colocalization Analyzer function in Fiji (21). All graphical representations and statistical analyses were carried out on Prism (v8.0.2, GraphPad, San Diego, CA) using two-way ANOVA with multiple comparisons.

CRISPR-mediated Knockout and Verification—Knockout cell lines were generated using the pSpCas9(BB)-2A-GFP (PX458) CRISPR/Cas9 construct (a gift from F. Zhang; Addgene, plasmid 4813 (22)) as described previously (4). In brief, CRISPR/Cas9 gRNAs were designed for gene-disruption using CHOPCHOP software (23). Transfections were performed using Lipofectamine LTX (ThermoFisher Scientific). Genomic DNA was isolated from each cell line and the targeted region amplified. PCR products were ligated into pGEM4Z expression vectors (24). Single clones were analyzed by Sanger sequencing. Indels for individual alleles are summarized in supplemental Table S1.

Mitochondrial Isolation—Mitochondria were isolated as previously described (25). Protein concentration was estimated by bicinchoninic acid assay (BCA) Pierce™ Protein Assay Kit (ThermoFisher Scientific).

Affinity Enrichment—Affinity enrichment assays were performed on knockout cell lines complemented with Flag-tagged cDNA. Briefly, WT and Flag-tagged whole cell pellets were harvested in triplicate. Pellets, representing 2.5 mg total protein, were re-suspended in Solubilization buffer (20 mM Tris-Cl pH 7.4, NaCl 50 mM, 10% glycerol, 0.1 mM EDTA) containing 1% digitonin (Merck, Darmstadt, Germany). Pierce™ Spin Columns (ThermoFisher Scientific) were loaded with 30 μl anti-Flag M2 affinity gel (Sigma) and equilibrated with Wash buffer (20 mM Tris-Cl pH 7.4, 60 mM NaCl, 10% glycerol, 0.5 mM EDTA) and 0.1% digitonin. Following clarification, solubilized proteins and complexes were added to the columns and incubated on a rotating mixer for 2 h at 4 °C. Columns were attached to a vacuum manifold and washed 20 times with 500 μl of Wash buffer. The columns were then incubated with 100 μl of elution buffer (Solubilization buffer plus 150 μg/ml Flag peptide) for 15 min at 4 °C before low speed centrifugation and collection into a microcentrifuge tube. This was repeated twice and the eluates were pooled. These were combined with 5× volumes (1 ml) of ice-cold acetone and the samples centrifuged at 14,000 × *g* for 10 min at 4 °C, following which the precipitated pellet was solubilized in 8 M urea and 50 mM ammonium bicarbonate. This was

sonicated in a water bath at room temperature for 15 min before addition of Tris(2-carboxyethyl)phosphine hydrochloride (TCEP) to a final concentration of 5 mM and chloroacetamide (Sigma Aldrich) to a final concentration of 50 mM and the sample was incubated at 37 °C while shaking. The sample was then treated with ammonium bicarbonate to dilute the urea to a final concentration of 2 M. Trypsin (1 μg; Promega, Madison, WI) was added to the sample before incubation overnight at 37 °C. After this the sample was acidified with 10% trifluoroacetic acid (TFA) to a final concentration of 1%. Stage tips were generated with two plugs of 3 M™ Empore™ SDB-XC Extraction Disks (Fisher Scientific, Pittsburgh, PA) that were activated with 100% acetonitrile (ACN) via centrifugation (26). All spins were performed at 1800 × *g*. The tips were washed with 0.1% TFA, 2% ACN three times. The sample was added to the stage tip and eluted with 80% ACN and 0.1% TFA. The eluates were subsequently dried down using a SpeedVac.

Mass Spectrometry of SILAC Treated Cells—Mitochondria were isolated as above from LYRM1^{KO}, LYRM9^{KO} and AltMiD51^{KO} cell lines cultured in SILAC DMEM and prepared as described previously (4). Analysis was performed on SILAC labeled whole cell lysates of the LYRM2^{KO} cell line. Mitochondrial protein yield and whole cell pellet protein amounts were assayed by BCA. For each triplicate set, two replicates containing 50 μg of protein from heavy labeled cells/mitochondria were mixed with the same amount of protein from light KO cells/mitochondria. The third replicate consisted of a label switch. Both whole cell and mitochondrial samples were treated as follows: samples were solubilized in 1% sodium deoxycholate, 100 mM Tris-Cl pH 8.1, 40 mM chloroacetamide and 10 mM TCEP before vortexing and heating for 5 min at 99 °C with 1500 rpm shaking. Samples were then sonicated for 15 min in a room temperature water bath before the addition of 1 μg trypsin (Promega) and incubation overnight at 37 °C. The supernatant was then transferred to 3 × 14G 3M™ Empore™ SDB-RPS stage tips (26). Ethyl acetate (99%) and 1% TFA was added to the tip before centrifugation at 3000 × *g* at room temperature as described (26). Stage tips were washed first with 99% ethyl acetate and 1% TFA and then with ethyl acetate supplemented with 0.2% TFA. Samples were eluted in 80% ACN and 1% NH_4OH, and acidified to a final concentration of 1% TFA before drying in a SpeedVac.

Mass-spectrometry and Data Analysis—Peptides were reconstituted in 2% ACN, 0.1% TFA and transferred to autosampler vials for analysis by online nano-HPLC/electrospray ionization-MS/MS on either a ThermoFisher Scientific Orbitrap Q Exactive Plus, Orbitrap Fusion Lumos Tribrid or Orbitrap Elite Hybrid Ion-Trap instrument as follows:

NDUFAB1^{Flag} and yACP1^{Flag} AE-MS were acquired on an Orbitrap Elite Hybrid Ion-Trap instrument connected to an Ultimate 3000 HPLC (ThermoFisher Scientific). Peptides were loaded onto a trap column (PepMap C18 trap column 75 μm × 2 cm, 3 μm, particle size, 100 Å pore size; ThermoFisher Scientific) at 5 μl/min for 3 min before switching the pre-column in line with the analytical column (PepMap C18 analytical column 75 μm × 50 cm, 2 μm particle size, 100 Å pore size; ThermoFisher Scientific). Peptide separation was performed at 300 nl/min using a 90 min non-linear ACN gradient of buffer A [0.1% formic acid, 2% ACN, 5% DMSO] and buffer B [0.1% formic acid in ACN, 5% DMSO]. Data was collected in Data Dependent Acquisition (DDA) mode using m/z 300–1650 as MS scan range, rCID for MS/MS of the 20 most intense ions. Other instrument parameters were: MS scan at 120,000 resolution, maximum injection time 150 ms, AGC target 1E6, CID at 30% energy for a maximum injection time of 150 ms with AGC target of 5000.

For LYRM2^{KO} whole cell SILAC measurements and LYRM2^{Flag} affinity enrichment, data was acquired on an Orbitrap Q Exactive Plus connected to an Ultimate 3000 HPLC. Peptides were loaded onto a trap column (Acclaim C18 PepMap nano Trap × 2 cm, 100 μm I.D, 5 μm particle size and 300 Å pore size; ThermoFisher Scientific) at 15 μl/min for 3 min before switching the pre-column in line with the analytical column (Acclaim RSLC C18 PepMap Acclaim RSLC nanocolumn 75 μm × 50 cm, PepMap100 C18, 3 μm particle size 100 Å pore size; ThermoFisher Scientific). The separation of peptides was performed at 250 nl/min using a non-linear ACN gradient of buffer A (0.1% formic acid, 2% ACN) and buffer B (0.1% formic acid, 80% ACN) over 280 min (LYRM2^{KO} whole cell) or 70 min (LYRM2^{Flag}). For LYRM2^{KO} analysis, data were collected in positive mode using Data Dependent Acquisition using *m/z* 375–1575 as MS scan range, HCD for MS/MS of the 12 most intense ions with charge ≥ 2. Other instrument parameters were: MS1 scan at 70,000 resolution (at 200 *m/z*), MS maximum injection time 54 ms, AGC target 3E6, normalized collision energy was at 27% energy, isolation window of 1.8 Da, MS/MS resolution 17,500, MS/MS AGC target of 2E5, MS/MS maximum injection time 54 ms, minimum intensity was set at 2E3 and dynamic exclusion was set to 15 s. For LYRM2^{Flag}, data were collected in positive mode using Data Dependent Acquisition using *m/z* 375–2000 as MS scan range, HCD for MS/MS of the 10 most intense ions with charge ≥ 2. Other instrument parameters were: MS1 scan at 70,000 resolution (at 200 *m/z*), MS maximum injection time 118 ms, AGC target 3E6, normalized collision energy was at 27% energy, isolation window of 1.8 Da, MS/MS resolution 35,000, MS/MS AGC target of 5E5, MS/MS maximum injection time 118 ms, minimum intensity was set at 5E3 and dynamic exclusion was set to 10 s.

For LYRM1^{KO}, AltMiD51^{KO}, and LYRM9^{KO} mitochondria, data were acquired on an Orbitrap Fusion Lumos instrument connected to an Ultimate 3000 HPLC. Peptides were loaded onto a trap column (PepMap C18 trap column 75 μm × 2 cm, 3 μm, particle size, 100 Å pore size; ThermoFisher Scientific) at 5 μl/min for 3 min before switching the pre-column in line with the analytical column (PepMap C18 analytical column 75 μm × 50 cm, 2 μm particle size, 100 Å pore size; ThermoFisher Scientific). The separation of peptides for was performed at 300 nl/min using a 90 min non-linear ACN gradient of buffer A [0.1% formic acid, 2% ACN, 5% DMSO] and buffer B [0.1% formic acid in ACN, 5% DMSO]. The mass spectrometer was operated in positive-ionization mode with spray voltage set at 1.9 kV and source temperature at 275 °C. Lockmass of 401.92272 from DMSO was used. Data were collected using the Data Dependent Acquisition using *m/z* 350–1550 at 120,000 resolution with AGC target of 5e5. The "top speed" acquisition method mode (3 s cycle time) on the most intense precursor was used whereby peptide ions with charge states ≥ 2–5 were isolated with isolation window of 1.6 *m/z* and fragmented with high energy collision (HCD) mode with stepped collision energy of 30 ± 5%. Fragment ion spectra were acquired in Orbitrap at 15000 resolution. Dynamic exclusion was activated for 30 s.

Raw files were analyzed using the MaxQuant platform (27) version 1.6.3.4 searching against the UniProt human database containing 20,399 reviewed, canonical entries (January 2019) and a database containing 246 common contaminants. For label-free (LFQ) AE-MS experiments, default search parameters were used with "Label free quantitation" set to "LFQ" and "Match between runs" enabled. In all cases, Trypsin/P cleavage specificity (cleaves after lysine or arginine, even when proline is present) was used with a maximum of 2 missed cleavages. Oxidation of methionine and N-terminal acetylation were specified as variable modifications. Carbamidomethylation of cysteine was set as a fixed modification. A search tolerance of 4.5 ppm was used for MS1 and 20 ppm for MS2 matching. False discovery rates (FDR) were determined through the target-decoy approach set to 1% for both peptides and proteins.

Using the Perseus platform (28) version 1.6.5.0, proteins group LFQ intensities were $\log_2$ transformed. Values listed as being "Only identified by site," "Reverse," or "Contaminants" were removed from the data set. Mitochondrial annotations were imported by matching with

the Mitocarta2 data set (29) by gene name and/or ENSG identifier. Experimental groups were assigned to each set of triplicates and the number of valid values for row group calculated. For each experiment (containing a control and an enrichment group) rows having less than 3 valid values in the enrichment group were removed and the missing values in the relevant control group imputed to values consistent with the limit of detection. Proteins identified from less than 2 unique peptides were excluded from further analysis. A modified two-sided *t* test based on permutation-based FDR statistics (28) was performed between the two groups. The negative logarithmic *p* values were plotted against the differences between the $\log_2$ means for the two groups. The significance threshold used for these experiments is noted in the relevant figure legend and supplementary tables. Non-mitochondrial proteins were removed based on their absence from MitoCarta 2.0, before plotting of the data. For SILAC experiments, default search parameters were used with multiplicity set to 2 (Lys8, Arg10) and "Match between runs" enabled. Using the Perseus platform (28) version 1.6.5.0, proteins group normalized H/L ratios were $\log_2$ transformed. Label switched samples (L/H) were inverted to KO/Control orientation before this step. Values listed as being "Only identified by site," "Reverse," or "Contaminants" were removed from the data set. Mitochondrial annotations were imported by matching with the Mitocarta2 data set (29) by gene name and/or ENSG identifier. Experimental groups were assigned to each set of triplicates rows with < 2 valid values for each group removed. A representative MS/MS spectra for each of the 17 proteins identified from a single peptide has been included in supplemental Fig. S4. Non-mitochondrial proteins were removed based on the absence of a Mitocarta 2.0 annotation, and a one sample Student's two-sided *t* test was performed within each group. The negative logarithmic *p* values were plotted against the differences between the mean ratios for each group. A significance threshold ($p < 0.05$) was used for all experiments. $\log_2$-transformed median SILAC ratios were mapped on homologous subunits of the respiratory chain complexes, mitoribosome assembly intermediate and mitoribosome. Applicable Protein Data Bank accession codes provided in text.

Experimental Design and Statistical Rationale—SILAC labeled whole cell and mitochondrial analyses were performed in triplicate, with a label switch as we have done previously (4, 30, 31). The statistical approaches used to analyze the data was consistent with published quantitative SILAC analyses from our (4, 31) and other labs employing similar instrumentation and methods. The $\log_2$ ratio values of proteins in replicates were normally distributed. The fold change threshold we used for significance was > 1.5 and a $p < 0.05$ following a single sample two-sided Student's *t* test. AE-MS analyses were performed in triplicate using label free quantitation and compared with untagged control cells as we (32) and others have done previously using similar instrumentation and methods. Imputation was performed only on values in controls and random values were drawn from a narrow distribution equivalent to the limit of detection of the instrument. The $\log_2$ intensity values of the proteins in replicate were normally distributed. Significantly enriched proteins were determined through a modified two-sided *t* test based on permutation-based FDR statistics (28) between the two groups, with an FDR of 1% and the s0 value determined iteratively to exclude any enriched proteins specific to the control group.

Protein Electrophoresis, In-Gel Activity Assays and Western Blot Analysis—SDS-PAGE samples were solubilized in LDS sample buffer (ThermoFisher Scientific) with 10 mM DTT and separated on Tris-Tricine 10–16% gradient gel as previously described (30, 33, 34). BN-PAGE and semi-dry western transfer was performed as described previously (35, 36). Blots were incubated with horseradish peroxidase coupled secondary antibodies and ECL chemiluminescent substrate (Bio-Rad, Hercules, CA) and immunoreactive bands detected using a Chemidoc XRS system (Bio-Rad). Bands were subsequently quantified using Image Lab (version 5.2.1; Bio-Rad). Antibodies were purchased for Core 1 (ThermoFisher, 16D10AD9AH5), NDUFV1 (Proteintech, Rosemont, IL; 11238–1-AP), MrpL45 (Sigma, HPA023373); Cox4 (Abcam, Cambridge, UK; ab110261), Flag M2 Clone (Sigma-Aldrich, F3165), ATP5A (Abcam, ab14748) and SDHA (Abcam, ab14715). Polyclonal rabbit antibodies were previously raised in-house for NDUFAF2 and NDUFA9 (37). Tom40 antibodies were a kind gift from M. Mori (Kumamoto). In-gel activity was performed as previously described (38).

Pulse Labeling of mtDNA-encoded Subunits—Labeling of mtDNA-encoded translation products with ^{35}S-Methionine/cysteine was performed as previously described (39). Isolated mitochondria were subjected to SDS-PAGE and transferred to PVDF membranes. Radiolabeled proteins were analyzed with an Amersham Biosciences Typhoon Gel and Blot Imaging System (GE Healthcare Life Sciences, Marlborough, MA).

Retroviral Transduction—Knockout cell lines were stably complemented via retroviral transduction as described previously (4, 40). Briefly, cDNA fragments were amplified from HEK293T RNA and sub-cloned into pBMN-Z (Addgene, 1764) in place of the LacZ cassette. HEK293T cells were transfected with retroviral constructs using Lipofectamine LTX (ThermoFisher Scientific). Resulting virus was harvested 72 h after infection. Viral particles were sterile filtered with 0.45 μm, PDVF membrane (Millipore, Burlington, MA) and supplied with 1 μg/μl polybrene addition to relevant knockout cell lines. Target cells were infected 24 h before the media was replaced. Stable cells were selected via addition of puromycin (2 μg/ml) for up to 72 h. Genomic DNA was isolated from candidate cell lines and the cDNA region amplified and sequence verified.

Oxygen Consumption Stress Test—Oxygen consumption and extracellular acidification rates were measured in live cells using a Seahorse Bioscience XFe-96 Analyzer. Briefly, 25,000 cells were plated per well in culture plates treated with 50 μg/ml poly-D-lysine. For each assay cycle, there were 4 measurements of 2 min mix, 2 min wait and 5 min measure. The following inhibitor concentrations were used: 2 μM oligomycin, 0.5 μM carbonyl cyanide m-chlorophenyl hydrazone (CCCP), 0.5 μM rotenone and 0.3 μM antimycin A. Data were normalized using the CyQUANT assay kit (Invitrogen, Waltham, MA) and analyzed using Wave2.6.0 and Prism (v8.0.2, GraphPad) software packages.

RESULTS

The NDUFAB1 Interactome—Previously, we generated a HEK293T cell line expressing a doxycycline inducible, Flag-tagged copy of NDUFAB1 (NDUFAB1^{Flag}) harboring CRISPR-mediated disruptions in the genomic wild-type *NDUFAB1* alleles (4). Cell viability was dependent on the addition of doxycycline (and thus NDUFAB1 expression), confirming the essential nature of the protein. To examine the role of NDUFAB1 in complex I, we also generated NDUFAB1 knockout cells rescued via the expression of the Flag-tagged yeast ACP (yACP1). Viability in this cell line was also dependent on addition of doxycycline, however complex I assembly and respiration were not restored (4). Based on these results, we concluded that the essential role of NDUFAB1 is separate to its role as a subunit of complex I. Affinity-enrichment quantitative mass spectrometry (AE-MS) on the NDUFAB1^{Flag} cell line, revealed a suite of mitochondrial proteins, including nine LYRM family members, to be enriched (Fig. 1*A*, 1*B*; supplemental Table S1). Many of these proteins were also detected

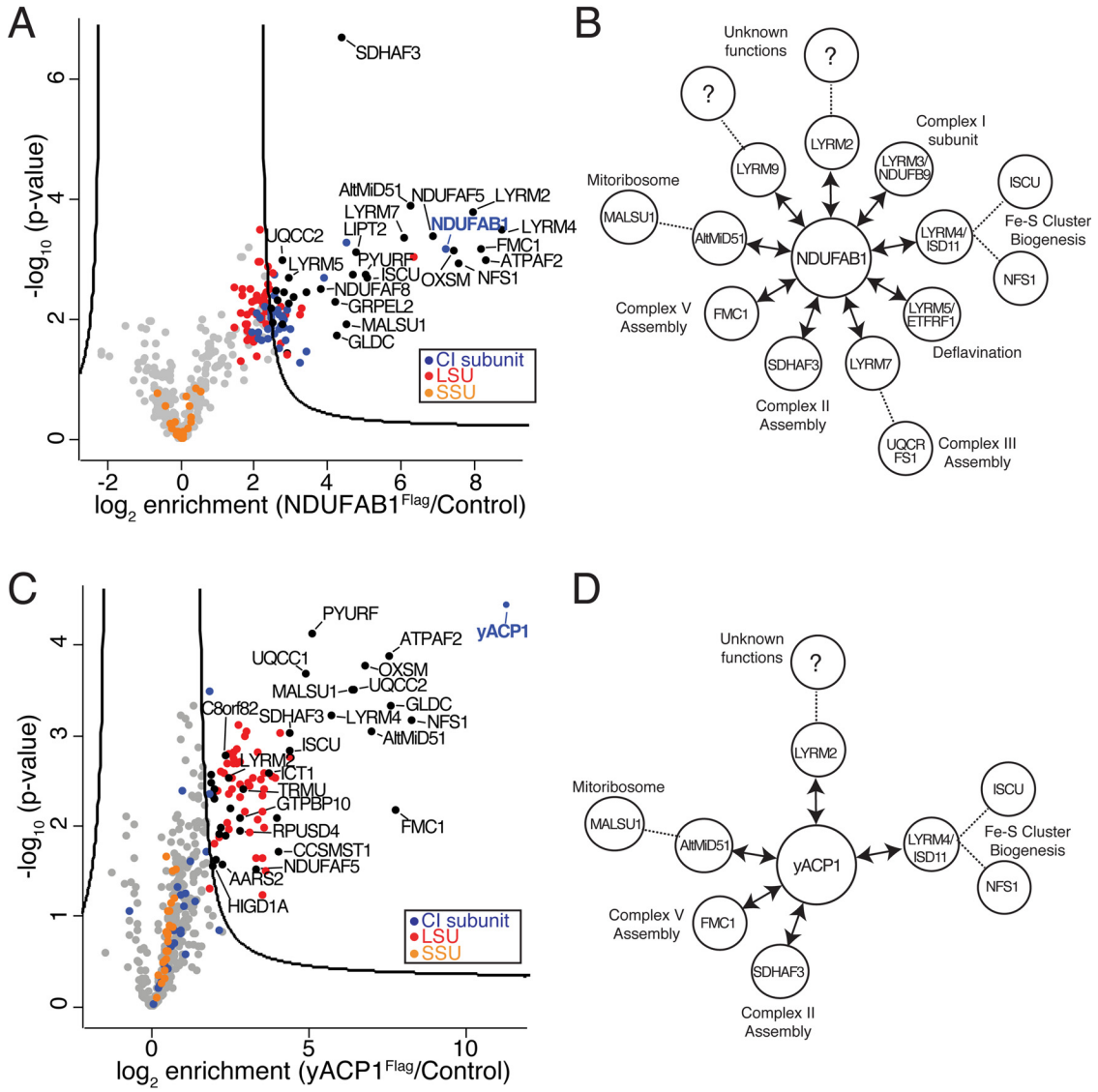

FIG. 1. **Determination of NDUFAB1 and yACP1 interactomes.** Affinity-enrichment mass spectrometry (AE-MS) were performed on (*A*) NDUFAB1^{Flag} cells and (*C*) yACP1^{Flag} cells. Following imputation of missing values for the control experiments, $\log_2$ transformed LFQ Intensities were submitted to a modified two-sided two-sample *t* test with significance determined by permutation-based FDR statistics (28). The negative logarithmic *p* values are plotted against the differences between the means for the two groups. A threshold of significance of $<$ 1% FDR @ s0 = 5 for panel *A* and 2 for panel *C* was determined as described in the methods. Schematic representation of LYRM-family proteins interacting with (*B*) NDUFAB1 and (*D*) yACP1. Enriched proteins known to interact with LYRM proteins and their associated pathways are shown in the outer ring.

in an independent study (41). To help determine which of these binding partners and associated mitochondrial processes are essential, AE-MS analysis was similarly performed on yACP1^{Flag} cells. This revealed the enrichment of five LYRM-family proteins (Fig. 1*C*, 1*D*; supplemental Table S1). Common to both was the association with LYRM4, which is involved in mitochondrial Fe-S cluster biogenesis (11, 33, 42). Other proteins involved in Fe-S cluster biogenesis (ISCU, NFS1) were also enriched, and this process is essential in eukaryotic cells including single-celled yeasts (43, 44). Taken together, it is likely that yACP1 complements the function of NDUFAB1 in this fundamental process, thereby leading to the survival of NDUFAB1 knockout HEK293T cells.

Analysis of Changes to the Proteome in LYRM^{KO} Cell Lines—LYRM2, a LYRM family member of unknown function, was also highly enriched in both the NDUFAB1 and yACP1 pull-downs and thus presented itself as an obvious candidate for further characterization. The LYRM member AltMiD51 was also highly enriched and we sought to clarify its functional importance in binding to the mitoribosome intermediate assembly (19). We also chose to interrogate the functions of the other uncharacterized LYRM-family members LYRM1 and

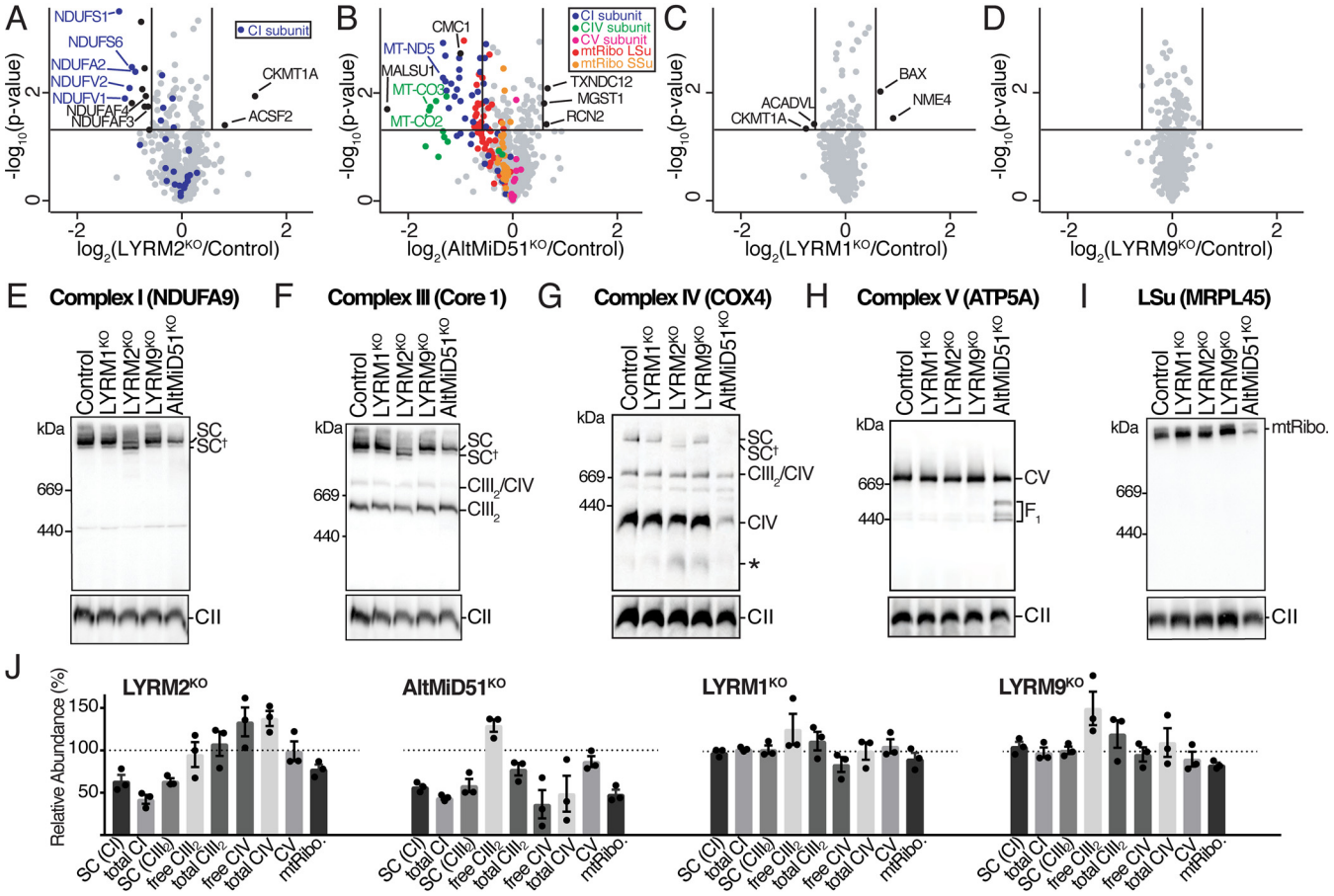

FIG. 2. **Proteomic and BN-PAGE analysis of select LYRM^{KO} lines.** Volcano plots demonstrating relative levels of proteins in (*A*) LYRM2^{KO}, (*B*) AltMiD51^{KO}, (*C*) LYRM1^{KO} and (*D*) LYRM9^{KO} cells. The mean of $\log_2$ transformed SILAC ratios for mitochondrial proteins detected for each KO against the HEK293T Control was analyzed by a single sample two-sided Student's *t* test and plotted against the negative $\log_{10}$ *p* value. $n = 3$ biological replicates. Dot colors as indicated. *E–I*, Mitochondria were isolated from control and KO cell lines, solubilized in 1% digitonin, subjected to BN-PAGE and immunoblottng with antibodies for (E) NDUFA9 (complex I), (*F*) Core 1 (complex III), (*G*) COX4 (complex IV), (*H*) ATP5A (complex V) and (*I*) MRPL45 (mitoribosome large subunit, LSu). Blots were re-probed with complex II subunit SDHA as loading control. SC, supercomplex; SC†, supercomplex assembly defect; $CIII_2$, complex III dimer, CIV, complex IV; mtRibo, mitoribosome; F_1, F_1-ATPase assemblies; asterisk, nonspecific complex; #, non-assembled COX4. (*J*) Mitochondrial complexes were quantified and shown as a percentage of control levels. SC(CI), SC($CIII_2$), free $CIII_2$, CV and mitoribosomal complex (mitoRibo) represent signals from digitonin-solubilized samples whereas total CI, total CIII and total CIV represent signals from Triton X-100 solubilized samples. Data shown as mean ± S.E., $n = 3$.

LYRM9, one of which (LYRM9), was enriched in the NDUFAB1 pull-down. We generated and validated HEK293T KO lines for LYRM1, LYRM2, LYRM9 and AltMiD51 via CRISPR/Cas9 mediated gene-editing (supplemental Table S2). AltMiD51 is located on a bicistronic transcript upstream of the mitochondrial fission receptor MiD51 (17) and has been found to be the main gene product (45). Western blot analysis verified that the mutations we generated did not interfere with downstream translation of MiD51 (supplemental Fig. S1). The validated clonal cell lines were subsequently subjected to SILAC (20) and quantitative MS analysis in order to determine the effect of each knockout on the proteome. Although loss of LYRM1 or LYRM9 appeared to have a minimal impact on the overall mitochondrial proteome, significant changes were observed following disruption of LYRM2 or AltMiD51 (Fig. 2*A*–2*D*; supplemental Table S3). LYRM2^{KO} whole cell proteomic analysis showed reduced levels of a subset of complex I subunits and assembly factors (Fig. 2*A*) along with a small number of proteins involved in one-carbon metabolism, nucleotide synthesis and protein import (supplemental Table S4). In the AltMiD51^{KO} cell line, subunits belonging to complex I, complex IV, the large subunit of the mitoribosome, as well as mitoribosome assembly factor MALSU1 were all reduced (Fig. 2*B*).

We used blue-native gel electrophoresis (BN-PAGE) and Western blot analysis to validate our findings. Mitochondria were isolated from control and each of the four KO cell lines, solubilized in digitonin and separated by BN-PAGE. Western blot analysis was performed using antibodies against each of the OXPHOS complexes and the large subunit of the mitori-

bosome (Fig. 2*E*–2*I*). Consistent with the proteomic analysis, a specific defect in the migration of the respiratory chain CI/$CIII_2$/CIV supercomplex (SC) was observed in LYRM2^{KO} mitochondria, resulting in a faster migrating form (indicated by SC† in Fig. 2*E*). When blots were incubated with antibodies specific to complex III (Fig. 2*F*) and complex IV (Fig. 2*G*), a similar defect was present in the supercomplex. Importantly, no changes in migration were present in the free complex III ($CIII_2$) and complex IV holoenzymes, nor the $CIII_2$/CIV complex, indicating that the defect was specific to complex I. Both complex V (Fig. 2*H*), and a mitoribosome complex containing large subunit protein MRPL45, appeared to migrate normally in LYRM2^{KO} mitochondria (Fig. 2*I*). Quantification of the levels of supercomplex and non-assembled free complexes from digitonin-solubilized samples, as well as the total levels of individual holo-complexes following Triton X-100 solubilization (which dissociates supercomplexes; supplemental Fig. S3), confirmed the complex I defect in LYRM2^{KO} mitochondria (Fig. 2*J*). An upregulation in complex IV was also observed and this has previously been observed in other HEK293T cells with complex I deficiency (4).

Strikingly, loss of AltMiD51 led to a decrease in the total abundance of the CI/$CIII_2$/CIV supercomplex and the CIV holoenzyme (Fig. 2*E*–2*G*). Defects were also seen for complex V, with the apparent accumulation of the F_1 module (Fig. 2*H*) (46). Consistent with broader defects in the OXPHOS machinery, loss of AltMiD51 led to reduced levels, but not a complete block in assembly of the mitoribosome (Fig. 2*I*). Quantification of complexes (Fig. 2*J*) showed the strong reduction in complexes I and IV. Interestingly the levels of free $CIII_2$ was increased in AltMiD51^{KO} cells, possibly reflecting the reduced formation of the supercomplex. A residual complex III dimeric pool has also been observed in mitochondria depleted of the general insertase OXA1L, even when other respiratory complexes were lost (47), suggesting that this dimeric form is a more stable entity. Quantification of complex III holoenzyme levels following Triton X-100 solubilization (supplemental Fig. S3) revealed a slight overall reduction in total levels (Fig. 2*J*). Total complex V levels were also like control. These results indicate that even though loss of AltMiD51 results in reduced levels of the mitoribosome, the individual OXPHOS complexes are differentially affected.

Given that LYRM1^{KO} and LYRM9^{KO} cells showed no strong defects at the proteomic level, nor defects in the assembly of major mitochondrial complexes responsible for OXPHOS (except for the apparent increase in complex III levels; Fig. 2*J*), we sought to verify that the LYRM members are resident mitochondrial proteins. Flag-tagged AltMiD51, LYRM1, LYRM2 and LYRM9 were re-expressed in their respective KO lines and subjected to immunofluorescence microscopy. In all cases, mitochondrial localization was clearly observed (supplemental Fig. S2*A* and S2*B*). We conclude that LYRM1 and LYRM9 may have redundant or condition-specific roles in mitochondria. We therefore chose to focus on AltMiD51 and LYRM2 for further characterization.

Loss of AltMiD51 Leads to Mitoribosome and Translation Defects—Using the proteomic data from AltMiD51^{KO} cells, a topographical proteomic heat-map was fitted onto the mature mitoribosome structure. This analysis clearly showed that the large subunit was specifically affected in AltMiD51^{KO} cells (Fig. 3*A*). Recently, the structure of a large subunit intermediate containing the assembly factor MALSU1, with AltMiD51 bound to NDUFAB1, was reported (19). When the relative abundance of individual proteins in AltMiD51^{KO} cells were mapped onto this structure, a reduction in all proteins found within the assembly intermediate was observed, as well as a particularly strong reduction in MALSU1 (Fig. 3*B*). This suggests that AltMiD51 is required for stabilization of MALSU1 during its role in mitoribosome assembly.

Topographical proteomic heat maps were also fitted onto the structures of each of the five OXPHOS complexes (Fig. 3*C*) (48–52). Consistent with the BN-PAGE results (Fig. 2), complexes I and IV were most affected by loss of AltMiD51, pointing to the importance of the hydrophobic mtDNA-encoded subunits for stability and structural integrity of the assembly modules (4, 53). Indeed, in our proteomics data set we could only detect three mtDNA-encoded subunits from complex I (ND5) and complex IV (CO2 and CO3). Each of these were the most reduced subunits in their respective complex upon loss of AltMiD51 (Fig. 2*B*). Although not significantly affected, subunits from complex V also trended toward protein turnover in the knockout, whereas subunits from complex II, the only respiratory chain enzyme not containing mtDNA-encoded subunits, were unaffected (Fig. 3*C*). To assess the translation of all mtDNA-encoded subunits, we performed pulse-labeling with [^{35}S]methionine. The AltMiD51^{KO} cells showed clear defects in the translation of subunits belonging to complex I (ND1, ND2, ND3, ND4L, ND5 and ND6), complex III (*Cyt* b) and complex IV (CO1, CO_2 and CO3) (Fig. 3*D*). Interestingly, translation of complex V subunits ATP6 and ATP8 were not reduced (see discussion). Pulse labeling of cells re-expressing Flag-tagged AltMiD51 led to an increase in the translation of most subunits compared with AltMiD51^{KO} cells and a concomitant reduction in ATP6 and ATP8. Partial rescue was only observed consistent with the incomplete restoration in the mitoribosome assembly (Fig. 3*E*) and may be because of insufficient expression levels of AltMiD51 or because of the Flag tag hindering activity. However, this rescue was enough to restore apparent steady-state supercomplex levels (Fig. 3*F*).

LYRM2 is Required for Complete Assembly of Complex I—Using the proteomic profile of LYRM2^{KO} mitochondria, we again prepared a topographical heat map of relative subunit ratios for complex I (Fig. 4*A*) (48). As can be seen, the levels of subunits belonging to the NADH-dehydrogenase (N-) module were strongly reduced whereas subunits belonging to the membrane arm were generally unaffected (Fig. 4*A* and 4*B*).

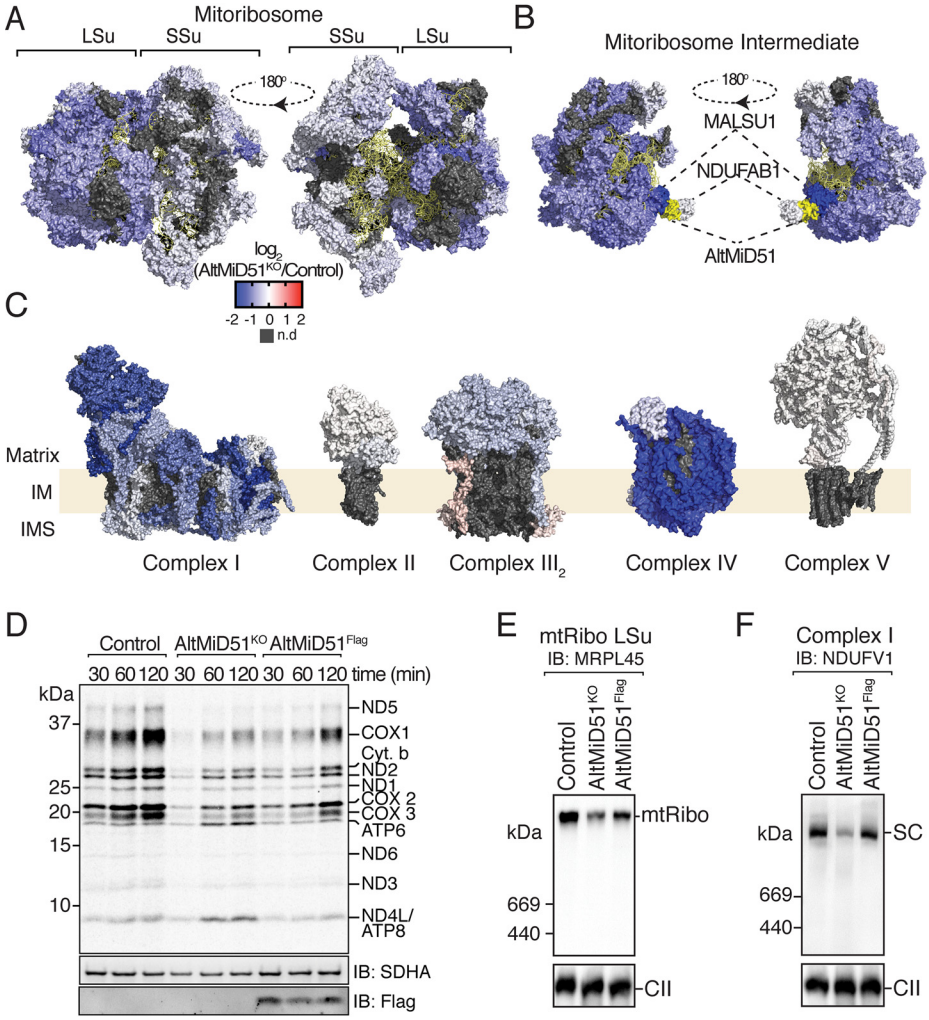

FIG. 3. **Analysis of mitoribosome and translation defects in AltMiD51^{KO} cells.** Topographical heat maps were fitted to the (*A*) mature mitoribosome (PDB: 3J9M (71)) and (*B*) stable assembly intermediate (PDB: 500L (19)). Blue is relatively less abundant, red is relatively more abundant, white is unchanged, dark gray is not detected and yellow is AltMiD51. rRNA is depicted in gold. C, Topographical heat-maps of the mitochondrial respiratory chain enzymes (complex I PDB: 5XTH (48), complex II PDB: 1ZOY (49), complex III dimer PDB: 1BGY (50), complex IV PDB: 5Z62 (72) and complex V PDB: 5ARE (52)). *D*, SDS-PAGE and phosphorimage analysis of ^{35}S-Met pulse labeled mtDNA subunits from control, AltMiD51^{KO} and AltMiD51^{KO} cells expressing AltMiD51^{Flag}. Immunoblotting using antibodies directed to the Flag epitope and SDHA were used as controls. *E*, Mitochondria were isolated from control, knockout and stably complemented cell lines, separated by BN-PAGE and assayed by Western blotting with antibodies against mitochondrial ribosome (MRPL45). CII serves as a loading control. *F*, As for E except probing for complex I (NDUFV1). LSu, large subunit; SSu, small subunit.

In our previous study, we generated KO cell lines specifically lacking the N-module of complex I (4). These cell lines had a faster migrating subcomplex consistent with that observed in LYRM2^{KO} mitochondria shown here. To analyze this in more detail, we investigated the assembly of the complex I holoenzyme using the stronger non-ionic detergent, Triton X-100, which dissociates supercomplexes into their holoenzyme forms (54). Complexes from control and LYRM2^{KO} mitochondria were subjected to BN-PAGE and Western blotting. Incubation with antibodies specific for the Q-module subunit NDUFA9 revealed the presence of a faster migrating species, consistent with loss of the N-module (Fig. 4*C*, CI$^{\Delta N}$). As it was unclear if the absence of the N-module was because of a defect in assembly, or a defect resulting in destabilization, we tested for the presence of NDUFAF2 within this complex. NDUFAF2 is a late-stage assembly factor which acts to stabilize the nascent complex I assembly intermediate but dissociates from the complex once the N-module is attached (37, 55). In this way, the presence of NDUFAF2 acts as a proxy for a complex I assembly intermediate devoid of the N-module. BN-PAGE analysis revealed that NDUFAF2 was stably associated with the CI$^{\Delta N}$ assembly in LYRM2^{KO} mitochondria whereas absent from control mitochondria (Fig. 4*D*). These results still do not discount the possibility that the CI$^{\Delta N}$ assembly present in LYRM2^{KO} cells represents a breakdown product that is subsequently stabilized by NDUFAF2. We therefore sought to test if this could be observed over a time course analysis where complex I was turned over. Control and LYRM2^{KO} cells were cultured in the presence of chloramphenicol (CAP), which arrests mitochondrial translation. As can be seen, the complex I-containing supercomplex in control cells was depleted over time (Fig. 4*E* left panel) but with no detection of a disassembled complex containing NDUFAF2 (right panel). In LYRM2^{KO} cells, the supercomplex lacking the N-module and containing NDUFAF2 was also depleted over time, showing the same kinetics as the fully assembled supercomplex in control cells (Fig. 4*E,* 4*F*).

It should be noted that in the absence of LYRM2, some fully assembled complex I was still present (42 ± 5%; Fig. 2*J*). A complex I in-gel activity assay confirmed that this complex contained an active NADH-dehydrogenase, and hence N-module (Fig. 5*A*). Nevertheless, a significant defect in basal

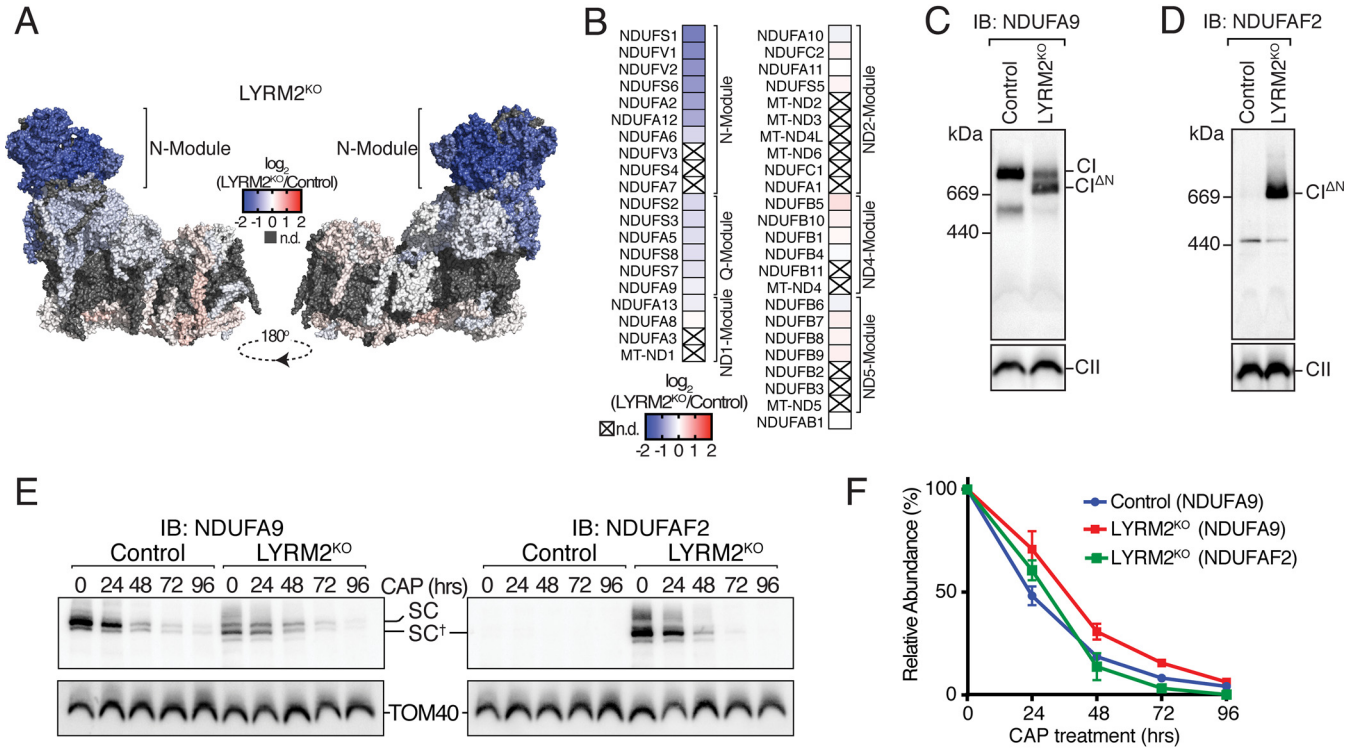

FIG. 4. **Defects in assembly of the complex I N-module in LYRM2^{KO} cells.** *A*, Topographical heatmap of proteomic analysis of LYRM2^{KO} fitted to the complex I structure. *B*, Heatmap showing relative decrease in abundance of each complex I subunit. "X" denotes undetected protein. *C–D*, Mitochondria from control and LYRM2^{KO} cells were solubilized in Triton X-100, subjected to BN-PAGE and Western blot analysis using antibodies against NDUFA9 and NDUFAF2 respectively. E, Mitochondria were isolated from cells grown in the presence of chloramphenicol (CAP) for the time indicated, solubilized in digitonin and subjected to BN-PAGE and Western blotting using antibodies directed to NDUFA9 or NDUFAF2. TOM40 (detecting the TOM complex) was used as a loading control. F, Data in (*E*) was quantified and shown relative to "0 h" for each sample. Data shown as mean ± S.D., $n = 3$.

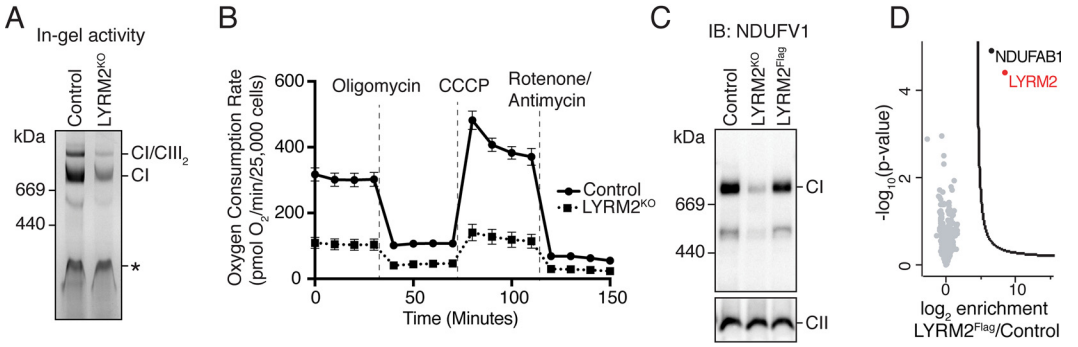

FIG. 5. **Loss of LYRM2 leads to respiration defects.** *A*, Mitochondrial proteins were separated by BN-PAGE before NADH-dehydrogenase in-gel activity assay; *, NADH dehydrogenase activity from dihydrolipoamide dehydrogenase (73). *B*, Oxygen consumption rates of control and LYRM2^{KO} cell lines using treatments as indicated. Data reported as mean ± S.D. $n = 8–9$. *C*, Mitochondria from control, LYRM2^{KO}, and LYRM2^{KO} cells stably complemented with Flag LYRM2^{Flag} were separated by BN-PAGE before Western blotting and incubation with antibodies against the complex I N-module subunit NDUFV1. *D*, AE-MS was performed on LYRM2^{Flag} whole cell lysates as in Fig. 1*A*. Threshold of significance of <1% FDR @ s0 = 1 was used, revealing specifically interacting proteins. Biological replicates $n = 3$. CI, complex I. CI$^{\Delta N}$, complex I missing N-module.

and maximal respiration was evident in LYRM2^{KO} cells indicating the importance of LYRM2 in normal mitochondrial respiration (Fig. 5*B*). Finally, the KO cell line was stably complemented with a Flag-tagged copy of LYRM2 (LYRM2^{Flag}). BN-PAGE analysis using antibodies against the N-module subunit NDUFV1 revealed rescue of the complex I assembly defect (Fig. 5*C*). We used the complemented cell line for immunoprecipitation and AE-MS analysis, revealing a strong interaction between LYRM2 and NDUFAB1 (Fig. 5*D*; supplemental Table S3). The lack of complex I subunits or assembly factors points to a transient interaction between these proteins during N-module assembly or integration.

DISCUSSION

LYRM-family proteins perform a variety of important functions within the mitochondrion (5, 11, 56, 57). These functions are executed via interactions with the soluble form of NDUFAB1 (8). As such, hypothesizing a function for any novel or otherwise uncharacterized LYRM protein solely on the presence of the tripeptide motif is unrealistic. Unbiased quantitative proteomic approaches in human KO cell lines were employed to obtain insights into potential roles of poorly characterized LYRM proteins. The absence of any notable changes in the protein profiles in either LYRM1^{KO} or LYRM9^{KO} cell lines is surprising, especially given their relatively uniform expression across different cell and tissue types (58). When our KO cell lines were complemented with Flag-tagged proteins and subjected to AE-MS analysis, there was very little co-enrichment of other mitochondrial proteins except for NDUFAB1 (data not shown). The lack of a strong phenotype for LYRM9 agrees with data from the International Knockout Mouse Consortium, which reports no phenotypic changes in a *Lyrm9*$^{-/-}$ mouse (59). No such data was available for LYRM1. We cannot rule out discrete and measurable functions for these proteins, such as in stress-induced, aged or environment-specific circumstances. For example, knockdown of LYRM1 in P19 mouse embryonic carcinoma cells have been reported to cause mitochondrial defects including reduced ATP levels and increased ROS production along with defects in differentiation and enhanced apoptosis (60). In the HEK293T cells used here, mitochondria and cell growth defects were not apparent. However, both LYRM1^{KO} and LYRM9^{KO} cell lines exhibited an increase in complex III levels which may indicate that loss of these proteins may impact on mitochondrial function leading to a compensatory mechanism in increased complex III assembly/stability. Clearer functionality, however, was evident from our studies of AltMiD51 and LYRM2.

AltMiD51 was earlier identified as an alternative transcript upstream of MiD51 (17), a protein involved in mitochondrial fission (61). AltMiD51 was also suggested to be involved in fission, with mutations in the LYR motif leading to mitochondrial elongation (17). However, it was more recently revealed that AltMiD51 indirectly bridges the connection between NDUFAB1 with a stable mitoribosome assembly intermediate via the assembly factor MALSU1 (19). Analysis of our AltMiD51^{KO} cells highlights the importance of AltMiD51 in optimal mitoribosome assembly. We observed reduced levels of the large mitoribosome subunit and its constituent proteins whereas proteins belonging to the small ribosomal subunit were not significantly reduced. Of note was the strong reduction in MALSU1 (c7orf30), a protein previously identified to be involved in biogenesis of the large mitoribosomal subunit (62–64). Our results are therefore consistent with AltMiD51 playing a role in mitoribosome assembly rather than acting in direct translational activation (18). Like that seen for knockout of AltMiD51 shown here, along with previous knockdown studies (18), knockdown of MALSU1 did not completely arrest mitoribosome biogenesis, nor translation of mtDNA encoded subunits (62–64). Nevertheless, AltMiD51^{KO} cells showed reduced levels of most mtDNA-encoded subunits and concomitant defects in the levels of respiratory chain complexes containing those proteins. Interestingly, ATP6 and ATP8 showed no translation defects during a pulse-labeling experiment, and this may reflect increased levels of their bicistronic transcript or translational activation because of the accumulation of the F_1-arm, as seen in yeast studies (65). Additionally, previous studies, including those involving knockdown of MALSU1 (62), have suggested that although a defect in mitochondrial translation will typically result in decreased levels of mitochondrial peptides, it can instead result in increased levels of some mtDNA-encoded proteins via apparent preferential translation of specific mRNAs (62, 66). Future targeted studies are required to investigate this possibility.

Topographical heat-map analysis of proteomic data also gave predictive insights into the importance of LYRM2 in OXPHOS and its function in assembly of the complex I N-module. This was confirmed by BN-PAGE Western blotting and in-gel activity and agrees with extensive data in the literature which suggests that the N-module is the final module to assemble (4, 67, 68). Given that complexes III and IV can still assemble with the complex lacking the N-module, our results also question conclusions made that the N-module integrates onto complex I before supercomplex assembly (67). Our results are also consistent with earlier findings that N-module assembly is not a prerequisite for supercomplex assembly (69). AE-MS studies were unable to elucidate other binding partners besides NDUFAB1, meaning the precise function of LYRM2 remains unclear. However, it is well established that LYRM2 is not a subunit of complex I and thus may be interacting with the N-module in a transient manner. Alternatively, it is possible that LYRM2 may be involved in the maturation of individual subunits such as incorporation of flavin mononucleotide (FMN) or Fe-S clusters that are present within the N-module. Several attempted approaches to uncover this transient interaction were unsuccessful but may depend on the metabolic status of the cell and acylation length of NDUFAB1 (8). Complete functionalization of LYRM2 in complex I assembly is an avenue for future research arising from our work.

Acknowledgments—We thank all Ryan lab members for ongoing input through experiment design and interpretation. We thank the Monash Micro Imaging facility and Monash FlowCore for their technical help and support. We thank the Bio21 Mass Spectrometry and Proteomics Facility and the Monash University Biomedical Proteomics Facility for the provision of instrumentation, training, and technical support. We acknowledge Bice Dibley for writing scripts for annotation and mapping of proteomics data onto PDB structures.

DATA AVAILABILITY

The mass spectrometry proteomics data have been deposited to the ProteomeXchange Consortium (http://proteomecentral.proteomexchange.org) via the PRIDE partner repository with the data set identifier PXD013706 (70).

* M.G.D. is supported by the Australian Mitochondrial Disease Foundation and an Australian Government Research Training Program Scholarship. F.K. is supported by a Monash University graduate research fellowship. We acknowledge funding from the National Health and Medical Research Council (NHMRC Project Grants 1164459 to M.T.R., 1125390, 1140906 to M.T.R. and D.A.S.; NHMRC Fellowship 1140851 to D.A.S.). The authors declare that they have no conflicts of interest with the contents of this article.

[S] This article contains supplemental Figures and Tables.

‖ These authors contributed equally to this work.

¶ To whom correspondence should be addressed. E-mail: Michael.Ryan@monash.edu.

Author contributions: M.G.D., L.E.F., F.K., D.A.S., and M.T.R. designed research; M.G.D., L.E.F., B.L., B.R., D.M., L.M.-W., F.K., A.J.S., D.A.S., and M.T.R. performed research; M.G.D., L.E.F., B.L., B.R., D.M., L.M.-W., F.K., A.J.S., D.A.S., and M.T.R. analyzed data; M.G.D., L.E.F., and M.T.R. wrote the paper.

REFERENCES

1. Hiltunen, J. K., Autio, K. J., Schonauer, M. S., Kursu, V. A., Dieckmann, C. L., and Kastaniotis, A. J. (2010) Mitochondrial fatty acid synthesis and respiration. *Biochim. Biophys. Acta* **1797,** 1195–1202
2. Maloney, F. P., Gerwick, L., Gerwick, W. H., Sherman, D. H., and Smith, J. L. (2016) Anatomy of the beta-branching enzyme of polyketide biosynthesis and its interaction with an acyl-ACP substrate. *Proc. Natl. Acad. Sci. U.S.A*. **113,** 10316–10321
3. Cronan, J. E., Fearnley, I. M., and Walker, J. E. (2005) Mammalian mitochondria contain a soluble acyl carrier protein. *FEBS Lett.* **579,** 4892–4896
4. Stroud, D. A., Surgenor, E. E., Formosa, L. E., Reljic, B., Frazier, A. E., Dibley, M. G., Osellame, L. D., Stait, T., Beilharz, T. H., Thorburn, D. R., Salim, A., and Ryan, M. T. (2016) Accessory subunits are integral for assembly and function of human mitochondrial complex I. *Nature* **538,** 123–126
5. Floyd, B. J., Wilkerson, E. M., Veling, M. T., Minogue, C. E., Xia, C., Beebe, E. T., Wrobel, R. L., Cho, H., Kremer, L. S., Alston, C. L., Gromek, K. A., Dolan, B. K., Ulbrich, A., Stefely, J. A., Bohl, S. L., Werner, K. M., Jochem, A., Westphall, M. S., Rensvold, J. W., Taylor, R. W., Prokisch, H., Kim, J. P., Coon, J. J., and Pagliarini, D. J. (2016) Mitochondrial protein interaction mapping identifies regulators of respiratory chain function. *Mol. Cell* **63,** 621–632
6. Angerer, H. (2013) The superfamily of mitochondrial Complex1_LYR motif-containing (LYRM) proteins. *Biochem. Soc. Transactions* **41,** 1335–1341
7. Runswick, M. J., Fearnley, I. M., Skehel, J. M., and Walker, J. E. (1991) Presence of an acyl carrier protein in NADH:ubiquinone oxidoreductase from bovine heart mitochondria. *FEBS Lett*. **286,** 121–124
8. Van Vranken, J. G., Nowinski, S. M., Clowers, K. J., Jeong, M. Y., Ouyang, Y., Berg, J. A., Gygi, J. P., Gygi, S. P., Winge, D. R., and Rutter, J. (2018) ACP acylation is an acetyl-CoA-dependent modification required for electron transport chain assembly. *Mol. Cell* **71,** 567–580.e4
9. Zhu, J., Vinothkumar, K. R., and Hirst, J. (2016) Structure of mammalian respiratory complex I. *Nature* **536,** 354–358
10. Fiedorczuk, K., Letts, J. A., Degliesposti, G., Kaszuba, K., Skehel, M., and Sazanov, L. A. (2016) Atomic structure of the entire mammalian mitochondrial complex I. *Nature* **538,** 406–410
11. Boniecki, M. T., Freibert, S. A., Mühlenhoff, U., Lill, R., and Cygler, M. (2017) Structure and functional dynamics of the mitochondrial Fe/S cluster synthesis complex. *Nat. Commun.* **8,** 1287
12. Van Vranken, J. G., Jeong, M. Y., Wei, P., Chen, Y. C., Gygi, S. P., Winge, D. R., and Rutter, J. (2016) The mitochondrial acyl carrier protein (ACP) coordinates mitochondrial fatty acid synthesis with iron sulfur cluster biogenesis. *Elife* **5,** pii: e17828
13. Na, U., Yu, W., Cox, J., Bricker, D. K., Brockmann, K., Rutter, J., Thummel, C. S., and Winge, D. R. (2014) The LYR factors SDHAF1 and SDHAF3 mediate maturation of the iron-sulfur subunit of succinate dehydrogenase. *Cell Metab.* **20,** 253–266
14. Sanchez, E., Lobo, T., Fox, J. L., Zeviani, M., Winge, D. R., and Fernández-Vizarra, E.. (2013) LYRM7/MZM1L is a UQCRFS1 chaperone involved in the last steps of mitochondrial Complex III assembly in human cells. *Biochim. Biophys. Acta* **1827,** 285–293
15. Lefebvre-Legendre, L., Vaillier, J., Benabdelhak, H., Velours, J., Slonimski, P. P., di and Rago, J. P. (2001) Identification of a nuclear gene (FMC1) required for the assembly/stability of yeast mitochondrial F(1)-ATPase in heat stress conditions. *J. Biol. Chem*. **276,** 6789–6796
16. Andreev, D. E., O'Connor, P. B., Fahey, C., Kenny, E. M., Terenin, I. M., Dmitriev, S. E., Cormican, P., Morris, D. W., Shatsky, I. N., and Baranov, P. V. (2015) Translation of 5′ leaders is pervasive in genes resistant to eIF2 repression. *Elife* **4,** e03971
17. Samandi, S., Roy, A. V., Delcourt, V., Lucier, J. F., Gagnon, J., Beaudoin, M. C., Vanderperre, B., Breton, M. A., Motard, J., Jacques, J. F., Brunelle, M., Gagnon-Arsenault, I., Fournier, I., Ouangraoua, A., Hunting, D. J., Cohen, A. A., Landry, C. R., Scott, M. S., and Roucou, X. (2017) Deep transcriptome annotation enables the discovery and functional characterization of cryptic small proteins. *Elife* **6,** pii: e27860
18. Rathore, A., Chu, Q., Tan, D., Martinez, T. F., Donaldson, C. J., Diedrich, J. K., Yates, J. R. 3rd, and Saghatelian, A. (2018) MIEF1 microprotein regulates mitochondrial translation. *Biochemistry* **57,** 5564–5575
19. Brown, A., Rathore, S., Kimanius, D., Aibara, S., Bai, X. C., Rorbach, J., Amunts, A., and Ramakrishnan, V. (2017) Structures of the human mitochondrial ribosome in native states of assembly. *Nat. Struct. Mol. Biol.* **24,** 866–869
20. Ong, S. E., Blagoev, B., Kratchmarova, I., Kristensen, D. B., Steen, H., Pandey, A., and Mann, M. (2002) Stable isotope labeling by amino acids in cell culture, SILAC, as a simple and accurate approach to expression proteomics. *Mol. Cell Proteomics* **1,** 376–386
21. Schindelin, J., Arganda-Carreras, I., Frise, E., Kaynig, V., Longair, M., Pietzsch, T., Preibisch, S., Rueden, C., Saalfeld, S., Schmid, B., Tinevez, J. Y., White, D. J., Hartenstein, V., Eliceiri, K., Tomancak, P., and Cardona, A. (2012) Fiji: an open-source platform for biological-image analysis. *Nat. Methods* **9,** 676–682
22. Ran, F. A., Lo, J. H., Rananaware, S., Downing, M., Panda, A., Tai, M., Raghavan, S., Fleming, H. E., and Bhatia, S. N. (2013) Genome engineering using the CRISPR-Cas9 system. *Nat. Protoc.* **8,** 2281–2308
23. Montague, T. G., Cruz, J. M., Gagnon, J. A., Church, G. M., and Valen, E. (2014) CHOPCHOP: a CRISPR/Cas9 and TALEN web tool for genome editing. *Nucleic Acids Res*. **42,** W401–7
24. Yanisch-Perron, C., Vieira, J., and Messing, J. (1985) Improved M13 phage cloning vectors and host strains: nucleotide sequences of the M13mp18 and pUC19 vectors. *Gene* **33,** 103–119
25. Johnston, A. J., Hoogenraad, J., Dougan, D. A., Truscott, K. N., Yano, M., Mori, M., Hoogenraad, N. J., and Ryan, M. T. (2002) Insertion and assembly of human tom7 into the preprotein translocase complex of the outer mitochondrial membrane. *J. Biol. Chem*. **277,** 42197–42204
26. Kulak, N. A., Pichler, G., Paron, I., Nagaraj, N., and Mann, M. (2014) Minimal, encapsulated proteomic-sample processing applied to copy-number estimation in eukaryotic cells. *Nature Methods* **11,** 319–324
27. Tyanova, S., Temu, T., and Cox, J. (2016) The MaxQuant computational platform for mass spectrometry-based shotgun proteomics. *Nat. Protoc.* **11,** 2301–2319
28. Tyanova, S., Temu, T., Sinitcyn, P., Carlson, A., Hein, M. Y., Geiger, T., Mann, M., and Cox, J. (2016) The Perseus computational platform for comprehensive analysis of (prote)omics data. *Nat. Methods* **13,** 731–740
29. Calvo, S. E., Clauser, K. R. and Mootha, V. K. (2016) MitoCarta2.0: an updated inventory of mammalian mitochondrial proteins. *Nucleic Acids Res*. **44,** D1251–D1257
30. Dibley, M. G., Ryan, M. T., and Stroud, D. A. (2017) A novel isoform of the human mitochondrial complex I subunit NDUFV3. *FEBS Lett.* **591,** 109–117
31. Stroud, D. A., Maher, M. J., Lindau, C., Vögtle, F. N., Frazier, A. E., Surgenor, E., Mountford, H., Singh, A. P., Bonas, M., Oeljeklaus, S., Warscheid, B., Meisinger, C., Thorburn, D. R., and Ryan, M. T. (2015) COA6 is a mitochondrial complex IV assembly factor critical for biogenesis of mtDNA-encoded COX2. *Human Mol. Gen.* **24,** 5404–5415
32. Lim, S., Tajika, M., Shimura, M., Carey, K. T., Stroud, D. A., Murayama, K., Ohtake, A., and McKenzie, M. (2018) Loss of the mitochondrial fatty acid β-oxidation protein medium-chain acyl-coenzyme A dehydrogenase disrupts oxidative phosphorylation protein complex stability and function. *Sci. Reports* **8,** 153

33. Cory, S. A., Van Vranken, J. G., Brignole, E. J., Patra, S., Winge, D. R., Drennan, C. L., Rutter, J., and Barondeau, D. P. (2017) Structure of human Fe-S assembly subcomplex reveals unexpected cysteine desulfurase architecture and acyl-ACP-ISD11 interactions. *Proc. Natl. Acad. Sci. U.S.A.* **114,** E5325–E5334
34. Schagger, H., and von Jagow, G. (1987) Tricine-sodium dodecyl sulfate-polyacrylamide gel electrophoresis for the separation of proteins in the range from 1 to 100 kDa. *Anal. Biochem.* **166,** 368–379
35. Formosa, L. E., Mimaki, M., Frazier, A. E., McKenzie, M., Stait, T. L., Thorburn, D. R., Stroud, D. A., and Ryan, M. T. (2015) Characterization of mitochondrial FOXRED1 in the assembly of respiratory chain complex I. *Human Mol. Gen.* **24,** 2952–2965
36. Wittig, I., Braun, H. P., and Schägger, H. (2006) Blue native PAGE. *Nat. Protocols* **1,** 418–428
37. Lazarou, M., McKenzie, M., Ohtake, A., Thorburn, D. R., and Ryan, M. T. (2007) Analysis of the assembly profiles for mitochondrial-and nuclear-DNA-encoded subunits into complex I. *Mol. Cell. Biol.* **27,** 4228–4237
38. Zerbetto, E., Vergani, L., and Dabbeni-Sala, F. (1997) Quantification of muscle mitochondrial oxidative phosphorylation enzymes via histochemical staining of blue native polyacrylamide gels. *Electrophoresis* **18,** 2059–2064
39. Formosa, L. E., Hofer, A., Tischner, C., Wenz, T., Ryan, M. T. (2016) Translation and assembly of radiolabeled mitochondrial DNA-encoded protein subunits from cultured cells and isolated mitochondria. *Methods Mol. Biol.* **1351,** 115–129
40. Morgenstern, J. P., and Land, H. (1990) Advanced mammalian gene transfer: high titre retroviral vectors with multiple drug selection markers and a complementary helper-free packaging cell line. *Nucleic Acids Res.* **18,** 3587–3596
41. Majmudar, J. D., Feng, X., Fox, N. G., Nabhan, J. F., Towle, T., Ma, T., Gooch, R., Bulawa, C., Yue, W. W., and Martelli, A. (2019) 4′-Phosphopantetheine and long acyl chain-dependent interactions are integral to human mitochondrial acyl carrier protein function. *Medchemcomm* **10,** 209–220
42. Shi, Y., Ghosh, M. C., Tong, W. H., and Rouault, T. A. (2009) Human ISD11 is essential for both iron-sulfur cluster assembly and maintenance of normal cellular iron homeostasis. *Hum. Mol. Genet.* **18,** 3014–3025
43. Lill, R., and Muhlenhoff, U. (2005) Iron-sulfur-protein biogenesis in eukaryotes. *Trends Biochem. Sci.* **30,** 133–141
44. Karnkowska, A., Vacek, V., Zubáčová, Z., Treitli, S. C., Petrželková, R., Eme, L., Novák, L., Žárský, V., Barlow, L. D., Herman, E. K., Soukal, P., Hroudová, M., Doležal, P., Stairs, C. W., Roger, A. J., Eliáš, M., Dacks, J. B., Vlček, Č., and Hampl, V. (2016) A eukaryote without a mitochondrial organelle. *Curr. Biol.* **26,** 1274–1284
45. Delcourt, V., Brunelle, M., Roy, A. V., Jacques, J. F., Salzet, M., Fournier, I., and Roucou, X. (2018) The protein coded by a short open reading frame, not by the annotated coding sequence, is the main gene product of the dual-coding gene MIEF1. *Mol. Cell Proteomics* **17,** 2402–2411
46. Vrbacky, M., Kovalèíková, J., Chawengsaksophak, K., Beck, I. M., Mráèek, T., Nùsková, H., Sedmera, D., Papoušek, F., Koláø, F., Sobol, M., Hozák, P., Sedlacek R., and Houštik, J. (2016) Knockout of Tmem70 alters biogenesis of ATP synthase and leads to embryonal lethality in mice. *Hum. Mol. Genet.* **25,** 4674–4685
47. Thompson, K., Mai, N., Oláhová, M., Scialó, F., Formosa, L. E., Stroud, D. A., Garrett, M., Lax, N. Z., Robertson, F. M., Jou, C., Nascimento, A., Ortez, C., Jimenez-Mallebrera, C., Hardy, S. A., He, L., Brown, G. K., Marttinen, P., McFarland, R., Sanz, A., Battersby, B. J., Bonnen, P. E., Ryan, M. T., Chrzanowska-Lightowlers, Z. M., Lightowlers, R. N., and Taylor, R. W. (2018) OXA1L mutations cause mitochondrial encephalopathy and a combined oxidative phosphorylation defect. *EMBO Mol Med*, **10,** pii: e9060
48. Gu, J., Wu, M, Guo, R., Yan, K., Lei, J., Gao, N., and Yang, M. (2016) The architecture of the mammalian respirasome. *Nature* **537,** 639–643
49. Sun, F., et al. (2005) Crystal structure of mitochondrial respiratory membrane protein complex II. *Cell* **121,** 1043–1057
50. Iwata, S., Huo, X., Zhai, Y., Wang, A., Xu, J., Su, D., Bartlam, M., and Rao, Z. (1998) Complete structure of the 11-subunit bovine mitochondrial cytochrome bc1 complex. *Science* **281,** 64–71
51. Shimada, S., Shinzawa-Itoh, K., Baba, J., Aoe, S., Shimada, A., Yamashita, E., Kang, J., Tateno, M., Yoshikawa, S., and Tsukihara, T. (2017) Complex structure of cytochrome c-cytochrome c oxidase reveals a novel protein-protein interaction mode. *EMBO J.* **36,** 291–300
52. Zhou, A., Rohou, A., Schep, D. G., Bason, J. V., Montgomery, M. G., Walker, J. E., Grigorieff, N., and Rubinstein, J. L. (2015) Structure and conformational states of the bovine mitochondrial ATP synthase by cryo-EM. *Elife* **4,** e10180
53. Mick, D. U., Fox, T. D., and Rehling, P. (2011) Inventory control: cytochrome c oxidase assembly regulates mitochondrial translation. *Nat. Rev. Mol. Cell Biol.* **12,** 14–20
54. McKenzie, M., Lazarou, M., Thorburn, D. R., and Ryan, M. T. (2007) Analysis of mitochondrial subunit assembly into respiratory chain complexes using Blue Native polyacrylamide gel electrophoresis. *Anal. Biochem.* **364,** 128–137
55. Ogilvie, I., Kennaway, N. G., and Shoubridge, E. A. (2005) A molecular chaperone for mitochondrial complex I assembly is mutated in a progressive encephalopathy. *J. Clin. Invest.* **115,** 2784–2792
56. Angerer, H., Radermacher, M., Mañkowska, M., Steger, M., Zwicker, K., Heide, H., Wittig, I., Brandt, U., and Zickermann, V. (2014) The LYR protein subunit NB4M/NDUFA6 of mitochondrial complex I anchors an acyl carrier protein and is essential for catalytic activity. *Proc. Natl. Acad. Sci. U.S.A.* **111,** 5207–5212,
57. Angerer, H. (2015) Eukaryotic LYR proteins interact with mitochondrial protein complexes. *Biology* **4,** 133–150
58. Uhlen, M., Fagerberg, L., Hallström, B. M., Lindskog, C., Oksvold, P., Mardinoglu, A., Sivertsson, Å., Kampf, C., Sjöstedt, E., Asplund, A., Olsson, I., Edlund, K., Lundberg, E., Navani, S., Szigyarto, C. A., Odeberg, J., Djureinovic, D., Takanen, J. O., Hober, S., Alm, T., Edqvist, P. H., Berling, H., Tegel, H., Mulder, J., Rockberg, J., Nilsson, P., Schwenk, J. M., Hamsten, M., von Feilitzen, K., Forsberg, M., Persson, L., Johansson, F., Zwahlen, M., von Heijne, G., Nielsen, J., and Pontén, F. (2015) Proteomics Tissue-based map of the human proteome. *Science* **347,** 1260419
59. Dickinson, M. E., Flenniken, A. M., Ji, X., Teboul, L., Wong, M. D., White, J. K., Meehan, T. F., Weninger, W. J., Westerberg, H., Adissu, H., Baker, C. N., Bower, L., Brown, J. M., Caddle, L. B., Chiani, F., Clary, D., Cleak, J., Daly, M. J., Denegre, J. M., Doe, B., Dolan, M. E., Edie, S. M., Fuchs, H., Gailus-Durner, V, Galli, A., Gambadoro, A., Gallegos, J., Guo, S., Horner, N. R., Hsu, C. W., Johnson, S. J., Kalaga, S., Keith, L. C., Lanoue, L., Lawson, T. N., Lek, M., Mark, M., Marschall, S., Mason, J., McElwee, M. L., Newbigging, S., Nutter, L. M., Peterson, K. A., Ramirez-Solis, R., Rowland, D. J., Ryder, E., Samocha, K. E., Seavitt, J. R., Selloum, M., Szoke-Kovacs, Z., Tamura, M., Trainor, A. G., Tudose, I., Wakana, S., Warren, J., Wendling, O., West, D. B., Wong, L., Yoshiki, A., International Mouse Phenotyping Consortium, Jackson Laboratory, Infrastructure Nationale PHENOMIN, Institut Clinique de la Souris (ICS), Charles River Laboratories, MRC Harwell, Toronto Centre for Phenogenomics, Wellcome Trust Sanger Institute, RIKEN BioResource Center, MacArthur, D. G., Tocchini-Valentini, G. P., Gao, X., Flicek, P., Bradley, A., Skarnes, W. C., Justice, M. J., Parkinson, H. E., Moore, M., Wells, S., Braun, R. E., Svenson, K. L., de Angelis, M. H., Herault, Y., Mohun, T., Mallon, A. M., Henkelman, R. M., Brown, S. D., Adams, D. J., Lloyd, K. C., McKerlie, C., Beaudet, A. L., Buæan, M., and Murray, S. A. (2016) High-throughput discovery of novel developmental phenotypes. *Nature* **537,** 508–514
60. Chen, Y. M., Li, X., Song, G. X., Liu, M., Fan, Y., Wu, L. J., Li, H., Zhang, Q. J., Liu, Y. Q., and Qian, L. M. (2016) Effect of LYRM1 knockdown on proliferation, apoptosis, differentiation and mitochondrial function in the P19 cell model of cardiac differentiation in vitro. *J. Bioenerg. Biomembr.* **48,** 33–41
61. Palmer, C. S., Osellame, L. D., Laine, D., Koutsopoulos, O. S., Frazier, A. E., and Ryan, M. T. (2011) MiD49 and MiD51, new components of the mitochondrial fission machinery. *EMBO Rep.* **12,** 565–573
62. Fung, S., Nishimura, T., Sasarman, F., and Shoubridge, E. A. (2013) The conserved interaction of C7orf30 with MRPL14 promotes biogenesis of the mitochondrial large ribosomal subunit and mitochondrial translation. *Mol. Biol. Cell* **24,** 184–193
63. Rorbach, J., Gammage, P. A., and Minczuk, M. (2012) C7orf30 is necessary for biogenesis of the large subunit of the mitochondrial ribosome. *Nucleic Acids Res.* **40,** 4097–4109
64. Wanschers, B. F., Szklarczyk, R., Pajak, A., van den Brand, M. A., Gloerich, J., Rodenburg, R. J., Lightowlers, R. N., Nijtmans, L. G., and Huynen,

M. A. (2012) C7orf30 specifically associates with the large subunit of the mitochondrial ribosome and is involved in translation. *Nucleic Acids Res.* **40,** 4040–4051

65. Rak, M., and Tzagoloff, A. (2009) F1-dependent translation of mitochondrially encoded Atp6p and Atp8p subunits of yeast ATP synthase. *Proc. Natl. Acad. Sci. U.S.A.* **106,** 18509–18514
66. Antonicka, H., Sasarman, F., Kennaway, N. G., and Shoubridge, E. A. (2006) The molecular basis for tissue specificity of the oxidative phosphorylation deficiencies in patients with mutations in the mitochondrial translation factor EFG1. *Human Mol. Gen.* **15,** 1835–1846
67. Guerrero-Castillo, S., Baertling, F., Kownatzki, D., Wessels, H. J., Arnold, S., Brandt, U., and Nijtmans, L. (2017) The assembly pathway of mitochondrial respiratory chain complex I. *Cell Metab.* **25,** 128–139
68. Formosa, L. E., Dibley, M. G., Stroud, D. A., and Ryan, M. T. (2018) Building a complex complex: Assembly of mitochondrial respiratory chain complex I. *Semin Cell Dev. Biol.* **76,** 154–162
69. Moreno-Lastres, D., Fontanesi, F., García-Consuegra, I., Martín, M. A., Arenas, J., Barrientos, A., and Ugalde, C. (2012) Mitochondrial complex I plays an essential role in human respirasome assembly. *Cell Metab.* **15,** 324–335
70. Perez-Riverol, Y., Csordas, A., Bai, J., Bernal-Llinares, M., Hewapathirana, S., Kundu, D. J., Inuganti, A, Griss, J, Mayer, G, Eisenacher, M., Pérez, E., Uszkoreit, J., Pfeuffer, J., Sachsenberg, T., Yilmaz, S., Tiwary, S., Cox, J., Audain, E., Walzer, M., Jarnuczak, A. F., Ternent, T., Brazma, A., and Vizcaíno, J. A. (2019) The PRIDE database and related tools and resources in 2019: improving support for quantification data. *Nucleic Acids Res*. **47,** D442–D450
71. Amunts, A., Brown, A., Toots, J., Scheres, S. H. W., and Ramakrishnan, V. (2015) Ribosome. The structure of the human mitochondrial ribosome. *Science* **348,** 95–98
72. Zong, S., Wu, M., Gu, J., Liu, T., Guo, R., and Yang, M. (2018) Structure of the intact 14-subunit human cytochrome c oxidase. *Cell Res.* **28,** 1026–1034
73. Yan, L. J., Yang, S. H., Shu, H., Prokai, L., and Forster, M. J. (2007) Histochemical staining and quantification of dihydrolipoamide dehydrogenase diaphorase activity using blue native PAGE. *Electrophoresis* **28,** 1036–1045